Infrared Ground-Based Astronomy with the Hughes 256 X 256 PtSi Array

A. Fowler, R. Joyce, and I. Gatley

National Optical Astronomy Observatories††
Tucson, Arizona 85726

J. Gates and J. Herring

Hughes Aircraft Company
Carlsbad, California

ABSTRACT

This paper will show that large format PtSi Schottky diode infrared arrays, the Hughes 256 X 256 hybrid Schottky array in particular, are competitive alternatives to the smaller format photovoltaic arrays for ground-based astronomy. The modest quantum efficiency of the PtSi compared to the photovoltaic devices is more than compensated for by the larger format. The use of hybrid technology yields effective fill factors of nearly 100%, and the low dark current, noise, excellent imaging characteristics, cost, and solid nitrogen operating temperature add to the effectiveness of this array for ground-based imaging. In addition to discussing the characteristics of this array, we will present laboratory test data and astronomical results achieved at Kitt Peak.

1. INTRODUCTION

Two dimensional platinum silicide (PtSi) Schottky barrier diode arrays have been utilized since the late 1970's. The early arrays[1-4] were burdened by poor fill factors due to their monolithic structure, in addition to the poor quantum efficiency of thick film PtSi. Since that time, very thin silicides utilizing optically reflective cavities, hybrid bump interconnect technology, and improved processing have dramatically improved the effective quantum efficiency, decreased the dark current, and increased the yield, making the present generation of arrays useful for ground-based astronomical applications.

This advance in technology has provided us with high performance arrays in the 256 X 256 format, with expectations of even larger formats in the future. This paper discusses the performance of the Hughes 256 X 256 PtSi array, which was tested by NOAO in cooperation with Hughes Aircraft Co. to evaluate its astronomical capabilities. The exciting characteristics of this array for astronomy are the large format, very low dark current, low noise, and ease of operation. Additional positive features are the cosmetic quality, stability of performance, and commercial availability.

2. DEVICE DESCRIPTION

Unlike most PtSi arrays, which are monolithic CCD's, this array utilizes hybrid technology. In this technique, the readout (ROIC) is fabricated using well-developed MOS technology and is tested separately before being mated with the detector. The detector array is also fabricated and tested independently. Indium bumps are defined on both the detector and readout, and those devices which pass the initial screening are then hybridized. Figure 1 is a cross section of a complete array, showing the hybrid structure. Besides the obvious benefits of increased yield and lower cost (since only good devices make it to the hybridization process), the fill factor is large because the readout does not reduce the detection area. This is very important in the case of Schottky devices because of their inherently lower quantum efficiency, and is crucial in any event for

††Operated by the Association of Universities for Research in Astronomy, Inc. under contract with the National Science Foundation.

astronomical use.

The ROIC uses a dual shift register addressing technique and a source follower per detector unit cell. The shift register is a two-phase non-overlapping clock design. Although the devices were designed to run at video rates, the shift registers will run as slow as 1 Hz when cooled to 60 K. This approach has the advantage of requiring fewer clocks, but the disadvantage of losing the ability to randomly access the pixels. This is not much of a practical loss, since the random access feature in other arrays has rarely been utilized.

The detector array, shown in cross-section in Figure 2, is a thin film PtSi structure. The array we evaluated incorporated a SiO dielectric optical cavity tuned to enhance the quantum efficiency at 4 microns, which unfortunately resulted in an optical null at 2 microns. This is not an intrinsic problem and is easily overcome by tuning the cavity differently, as shown later. Elabd and Kosonocky[5] provide a readable treatment of the use of optical cavities in thin film PtSi.

The principle of Schottky diode detection is the internal photoemission of hot holes created by the absorption of a photon. The incoming photon excites electrons in the valence band to energies above the Fermi level, creating holes below the Fermi level. A hot hole, one whose energy is above the Schottky barrier level, can tunnel into the detector substrate. An additional constraint for hot hole tunneling is that its momentum normal to the silicide-silicon surface correspond to an energy greater than the Schottky potential. The use of a dielectric on the backside of the silicide increases the probability of hot hole injection by scattering at this surface and significantly improves the quantum efficiency of these devices.

The fabrication of an extremely uniform silicide layer, as well as the lack of differential thermal contraction between the detector and ROIC, make possible physically large arrays with excellent cosmetic quality. Figure 3 is a ratio of two dome flats (4 s and 2 s integration time), displayed over the range 1.9 - 2.1. With the exception of the upper left corner, where the bonding to the detector substrate is made, only a few pixels were non-operative.

3. ASTRONOMICAL PERFORMANCE

The arrays described here were evaluated in the laboratory, with emphasis on those characteristics important for astronomical applications. Critical factors include (but are not limited to) dark current, read noise, quantum efficiency, linearity, and stability. One of the arrays was used on several occasions at Kitt Peak National Observatory to evaluate its performance under actual observing conditions; these results are discussed in the following section. The characterization and telescope tests were all at a detector temperature of approximately 60K, a temperature attained by pumping on LN_2, obviating the need for LHe and reducing the cost and complexity of operation.

After optimization for slow scan operation, the conversion gain (volts/electron) was determined using the "mean-variance" technique of Fowler and Joyce[6]. Following this, we determined the electrical gain by varying the reset voltage on the detector, obtaining a value of 14 electrons/ADU at the detector node. We could then calculate the capacitance of the detector and the system readout noise in electrons. The physical and derived detector characteristics are given in Table 1. Although the node capacitance is small, we were able to use a large reset level (3 V) to obtain a theoretical well capacity of ~ 10^6 electrons. In practice, the high conversion gain and the 16-bit A/D limited the practical capacity to about 3 X 10^5 electrons, which nonetheless gave excellent dynamic range due to the low read noise. The low node capacitance is largely repsonsible for the very low read noise, although this array, like others we have tested, appears to generate considerable noise in the addressing operation itself.

Table 1 -- Detector Characteristics

• HFPA Structure	
Number of Pixels	256 X 256; 65536 elements
Pixel Size	30 μm X 30 μm
Detector Active Area	28 μm X 28 μm
Readout Type	Direct Readout
Sensor Type	PtSi Schottky Barrier (C_1 = 0.29 / eV; Ψ_{ms} = 0.22 eV)
• HFPA Performance	
Operating Temperature	60 K
Dark Current	< 10 electron/s
Noise	40 electrons
Node Capacitance	0.06 pF
Full Well (3 V reset)	~ 1 X 10^6 electrons

The specific readout technique used presently deserves mention at this point. A common method, which we have used in the past, is to perform the address cycle (read signal, reset detector, read bias) on a sequential pixel-by-pixel basis, as illustrated in Figure 4a. With this data, the user can perform delta-reset, correlated double sampling, or correlated triple sampling operations[7]. Each of these techniques addresses different fundamental noise sources. However, our experience has indicated that the limiting performance is determined not by fundamental noise processes, but by excess noise associated with the addressing cycle. An alternative technique, illustrated in Figure 4b, is to perform a detector reset (only) on the entire array, followed by a readout of the entire array, without resetting (initial detector bias). After a delay for the desired integration time, the array is read out again (signal). The difference between the two values is the measured signal. This is a form of non-destructive double correlated sampling, but its most important feature is the elimination of excess noise associated with the resetting process. Using this technique, we have routinely achieved a read noise of 40 electrons with these PtSi arrays. The use of triple correlation to remove some of the 1/f noise may lead to further improvement, but we have not investigated this at present.

The dark current in this array, measured over time periods from 0.4 to 4000 seconds, is slightly higher for integration times less than 100 s (approximately 10 electrons/s), decreasing to about 3 electrons/s at longer integration times. Since these values are much lower than the background radiation flux for broadband imaging applications, little additional testing was done. We point out that due to the lower quantum efficiency of Schottky diodes, the dark current must be proportionally lower to avoid degrading the performance.

A key parameter for all detectors is the quantum efficiency. Two different arrays were tested in this effort. The first was optimized for thermal imaging with an anti-reflection coating and optical cavity tuned for 4 microns. This had the unfortunate consequence of severely reducing the quantum efficiency at 2 microns. The second array, with a different optical cavity, had a quantum efficiency almost 10 times higher at 2 microns. The measured quantum efficiencies of the two detectors as a function of wavelength are plotted in Figure 5, along with the theoretical performance predicted by a modified "Fowler" equation[7]. The theoretical response utilizes parameters determined from behavior in the 3 - 5 micron range and does not include the effects of transmission through the Si substrate, and thus overestimates the quantum efficiency at shorter wavelengths.

The effective optical fill factor of an array (which may be greater than the geometrical fill factor) is of paramount importance to astronomy. It determines the effective quantum efficiency for an array, which is the measured flux divided by the incident flux per area defined by the pixel center- to-center spacing. More importantly, a near 100% fill factor is necessary for stellar imaging, or signal variations due to the image centroid position relative to the centroid of the pixel point spread function (PSF) cannot be corrected. Pixel-to-pixel gain variations may be calibrated by uniform illumination of the array (flatfielding). The pixel PSF was evaluated in the laboratory by scanning a spot image (~ 20 microns) along a row of the array. The measured response for each of three adjacent pixels as a function of the spot position is plotted in Figure 6, along with the sum of the response. The lack of a statistically measurable dip at the interstitial positions leads us to conclude that the fill factor of this array is essentially 100%.

It is instructive to compare the performance of the PtSi array with that of the SBRC InSb array on a pixel basis. Figure 7a shows the calculated signal and noise, using typical values for InSb (η = 0.6, N_R = 300 electrons) and PtSi (η = 0.05, N_R = 40 electrons), for a photon flux = 1000 /s at a wavelength of 2.2 microns, as a function of the integration time. Complete linearity is assumed. The solid lines represent the measured signal (electrons) for the two detectors. The dashed lines represent the measured noise (electrons), under the assumption that the only noise sources are the read noise N_R and the shot noise of the radiation signal. The arrows indicate equal contributions from these two noise sources and mark the transition from "read noise limited" to "background limited" operation. The ratio of the signal/noise for InSb to that of PtSi, which may be considered the relative performance, is plotted in Figure 7b. The read noise limited regime corresponds to observations through very narrow spectral filters or applications such as speckle, where the integration time must be limited. The signal/noise is directly proportional to integration time and the ratio η/N_R. The much lower read noise of PtSi almost compensates for its lower quantum efficiency. Almost all astronomical imaging falls in the other, background limited, category. The signal/noise in this regime is independent of read noise, depending only on $(\eta)^{0.5}$, giving the InSb an advantage of 3.5, or about 1.4 magnitudes in sensitivity for a given integration time. Alternatively, the PtSi will require a factor of 12 greater integration time to reach the same signal/noise as the InSb. For applications requiring coverage of a large spatial area, this is more than compensated for by the pixel ratio of 18 between the 256 X 256 and 58 X 62 arrays.

An interesting parameter derived from Figure 7a, the integration time to background limited performance (shown by arrows), scales as $(N_R)^2/(\eta)$, and is more than a factor of 4 less for the PtSi than for the InSb. In the background limited regime, no theoretical advantage distinguishes a small number of long integrations from a large number of short integrations, as long as the total integration time is the same. Under the time-dependent sky background conditions encountered in actual observing, the ability to reach background limited conditions quickly may permit greater suppression of systematic effects, more than compensating for the slight increase in overhead associated with shorter integrations.

4. OBSERVATIONAL RESULTS

For the astronomical tests, input optics were installed in the cryostat to convert it to an uplooking camera very similar to that used at KPNO with the 58 X 62 SBRC InSb array.[8] To exploit fully the wide field capabilities of the PtSi array, the telescope focal plane was reduced in scale by a factor of 4, using AR-coated ZnSe lenses. The optical path was similar to that illustrated in Figure 8 of Fowler *et al.*[8] The optics consisted of a field lens near the telescope focal plane to reimage the exit pupil on a cold stop and a triplet in front of the array to achieve the focal reduction. The resulting plate scale on the KPNO 1.3m telescope was 1.36 arcsec/pixel, yielding a field of view 350 arcsec square. At the KPNO 2.1m telescope, the corresponding numbers are 0.78 arcsec/pixel and a 200 arcsec field.

Initial linearity observations were very encouraging. Figure 8 plots the integrated signal in a 5 pixel radius aperture for three stars at integration times ranging from 0.4 to 500 s. The dashed lines have a slope of 1.0. No significant deviation from linearity was seen for the two fainter stars; the deviation in the case of HR 5447 results from saturation of the electronics for the brightest pixels in the stellar image. The calculated intensity differences for the three stars are equal, within the quoted uncertainty, to published values.

A striking example of the performance of this device is shown in Figure 9, a K band image of the galactic center. This image is a mosaic of 25 exposures, each of 3 minutes, taken on 5 arcmin centers, and required approximately 1.5 hours of observing time at the 1.3m telescope. In this and succeeding images, north is up and east is to the left. The field of Figure 9 is approximately 27 arcmin on a side, or 70 pc at the distance of the galactic center. The nucleus is prominent in the center, and thousands of stars, as faint as K = 14, are detected. In addition, the plane of the galaxy, which runs from upper left to lower right, is evident, as is the patch of extinction running parallel to and slightly below the plane, which indicates that our solar system actually lies somewhat above the galactic plane. The patch of extinction about 10 arcmin NW of the center is almost devoid of stars even at this wavelength, suggesting that it is both very thick optically and nearby. Since the visual extinction to the galactic center is estimated to be 15 - 20 mag, almost none of the thousands of stars in this image is detectable at visual wavelengths.

The linear artifact seen on the left side of Figure 9 results from a bright star falling on the edge of the detector-ROIC hybrid interface. Some of this radiation channels across the array within the optical cavity. This effect can easily be prevented by optical masking of the array.

A similar artifact, resembling diffraction spikes along the row and column directions, can be seen surrounding very bright stars. This effect was seen only at K with the array tuned for 4 micron operation and probably is a result of the detuned optical cavity acting as a waveguide and channelling some of the light from the stellar image down the rows and columns of the array. This should not be a significant effect in an array with a properly tuned optical cavity.

Figure 10 is a single frame image (24 coadded 10s integrations) of the Orion Nebula through a 3.28 micron narrowband ($\Delta\lambda$ = 0.1 micron) filter, which isolates the "PAH" emission feature[9,10], a tracer of "hot" dust near sources of ultraviolet radiation. This image prominently illustrates the concentration of this feature along the ionization front of the nebula,[11,12] and shows that PtSi is adequate for many observations longward of 3 microns. Although the theoretical advantage of the much higher quantum efficiency of InSb is considerable in this region, the practical advantage in this "saturation limited" regime is constrained by the finite readout time for the array. The 58 X 62 InSb array in use at NOAO will saturate in the L band filter in approximately 0.1s; a hypothetical 256 X 256 array in this material would require operation at much higher detector bias and clock rate, or through a narrowband filter, to avoid saturation in the minimum integration time. Except for scientific applications requiring narrowband imaging, the low quantum efficiency of PtSi in the L and M bands is compensated for by the ability to use broadband filters.

Figure 11 is a large mosaic image of the region of the Orion Nebula in the H band. The field of view is approximately 27 by 37 arcmin. The familiar shape of the Orion Nebula in the visible, largely the result of dust obscuration, is modified in the infrared to a more symmetrical form. In addition to the Trapezium and the OMC1 complex, one may trace a distribution of stars clusters extending to the north, including the OMC2 complex and a previously unknown bipolar outflow object. This type of image gives a global view of the large and small scale details of star formation in a way impossible before the advent of large-format sensitive infrared arrays.

The construction of mosaic images such as these requires a detector with excellent long-term stability in its spatial sensitivity characteristics, since the effects of temporally varying sky emission must be removed from the individual images prior to coalescence. This is accomplished by using median-averaged frames of off-object "sky", or the object frames themselves, if the star density is low enough, to generate a flatfield frame, essentially a spatial gain map of the array using the sky background emission as a uniform illumination source. Dividing the object frames by this flatfield reduces the sky background in each frame to a constant, which can be subtracted in the mosaic operation. Any variation in the spatial gain over the array during the observations will be manifested as discontinuities in the mosaic, since it will be impossible to match the levels at more than one border. The lack of such features in Figures 9 and 11 attests to the excellent stability of the PtSi array.

An additional consideration for mosaic observations is the need to overlap adjacent frames to obtain a common area for spatial registration and sky level matching. The area of this overlap region will depend on star density and telescope pointing errors, and will be a smaller fraction of the field of view for a larger format array. In addition, covering a given sky area with a small field of view requires that a greater fraction of time be spent in overhead operations, such as moving the telescope. The net result is that for actual mapping operations, the advantage of a large format array is considerably greater than the numerical pixel ratio.

5. SUMMARY

In this paper we have shown the capabilities and utility of PtSi large format arrays. Although their ultimate sensitivity is a factor of 3 to 4 less than the most sensitive photovoltaic arrays, the larger format, stable characteristics, and lower cost make them very attractive, competitive devices for ground-based astronomy.

The comparisons we have made between the 256 X 256 PtSi and the 58 X 62 InSb arrays indicate that they may play complementary roles in astronomy. Certainly, for deep limit observations of distant galaxies or faint stars, the sensitivity advantage of the InSb is of paramount importance. One cannot realistically overcome this fact by a 12-fold increase in observing time, especially on 4 meter class telescopes. However, as pointed

out above, the numerical pixel advantage can more than compensate for the sensitivity factor in observations of extended fields. In addition, our experience indicates that it is very difficult to accurately mosaic extended objects with a limited field of view that does not include "sky", without significant spatial oversampling. A final point lies in the value of large format arrays on moderate aperture telescopes for serendipitous discovery and the necessary survey work prior to deep imaging or spectroscopy on existing 4m and future 8m and 10m class telescopes.

6. ACKNOWLEDGEMENTS

We wish to acknowledge the efforts of K. M. Merrill and M. Tamura in generating the composite image of the Orion Nebula, H. Chen for performing the spot scan tests, and Kate McKennon for the drawings. We thank J. Mooney of RADC for permission to publish his quantum efficiency measurements of one of the arrays. L. Davis generated the IRAF routines which made possible the mosaic images presented here.

REFERENCES

1. F. D. Shepherd, A. C. Yang, S. A. Roosild, J. H. Bloom, B. R. Capone, C. E. Ludington, and R. W. Taylor 1976, "Silicon Schottky Barrier Monolithic IRTV Focal Planes," *Advances in Electronics and Electron Physics*, **40B**, pp. 981-992.
2. F. D. Shepherd, R. W. Taylor, L. H. Taylor, L. H. Skolnik, B. R. Capone, S. A. Roosild, W. F. Kosonocky, and E. S. Kohn 1979, "Schottky IRCCD Thermal Imaging ," *Advances in Electronics and Electron Physics*, **52**, pp. 495-512.
3. W. F. Kosonocky, H. Elabd, H. G. Erhardt, F. V. Shallcross, G. M. Meray, R. Miller, T. S. Villani, J. V. Groppe, V. L. Frantz, and F. J. Tams, "Schottky-barrier Infrared Image Sensors," *RCA Engineer* **27-3**, (May/June 1982).
4. B. R. Capone, R. W. Taylor, and W. F. Kosonocky 1982, "Design and Characterization of a Schottky Infrared Charge Coupled Device (IRCCD) Focal Plane Array," *Optical Engineering*, **21**, 945.
5. H. Elabd and W. F. Kosonocky, "Theory and Measurements of Photoresponse for Thin Film Pd_2Si and PtSi Infrared Schottky-Barrier Detectors with Optical Cavity," *RCA Review* **43** (Dec 1982).
6. A. Fowler and R. Joyce, "Status of the NOAO Evaluation of the Hughes 20 X 64 Si:As Impurity Band Conduction Array," this proceedings (Feb 1989).
7. A. Fowler, R. Joyce, I. Gatley, J. Gates, and J. Herring 1989, "Evaluation of a 256 X 256 PtSi Array for Infrared Ground-Based Astronomy," *SPIE Infrared Detectors, Focal Plane Arrays, and Imaging Sensors*, **1107-06**.
8. A. M. Fowler, Ian Gatley, F. Stuart, R. R. Joyce, and R. G. Probst 1988, "National Optical Astronomy Observatories 1-5 Micron Imaging Camera: A New National Resource," *SPIE Infrared Technology XIV*, **972**, 107.
9. R. W. Russell, B. T. Soifer, and S. P. Willner 1977, *Ap. J. (Letters)*, **217**, L149.
10. L. J. Allamandola, A. G. G. M. Tielens, and J. R. Barker 1985, *Ap. J. (Letters)*, **290**, L25.
11. K. Sellgren 1981, *Ap. J.*, **245**, 138.
12. I. Gatley and N. Kaifu 1985, "Infrared Observations of Interstellar Molecular Hydrogen," *IAU Symposium No. 120*, ed. Vardya and Tarafdar, p. 153.

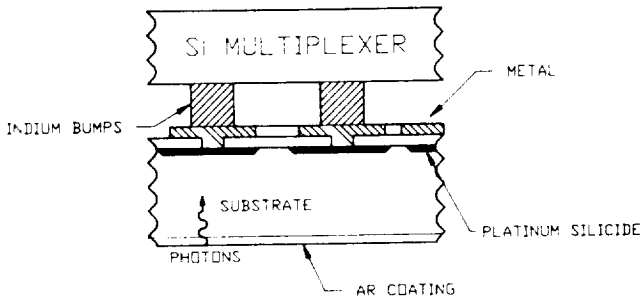

HYBRID ARRAY CROSS SECTION

Figure 1.

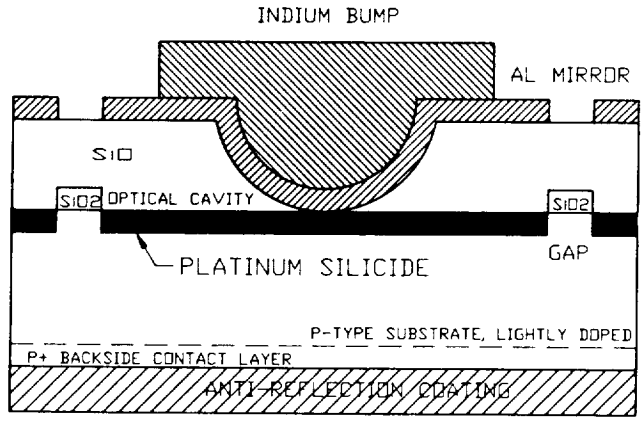

Pt Si ARRAY PIXEL CROSS SECTION

Figure 2.

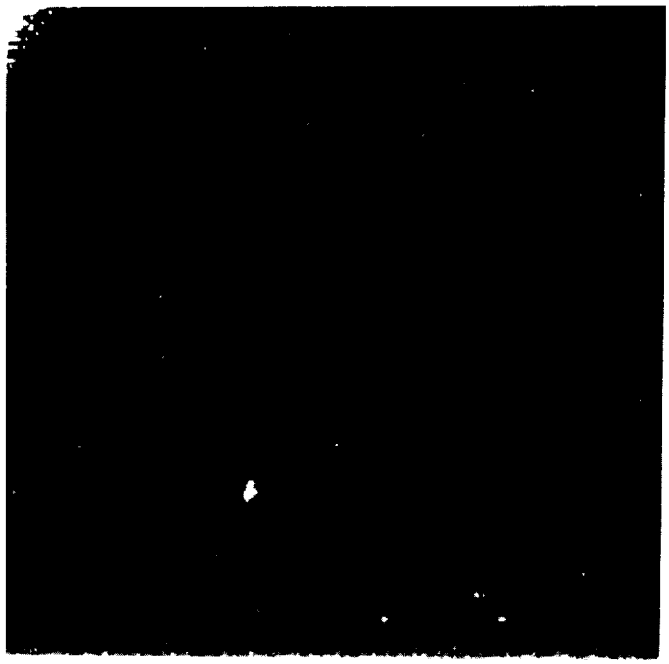

Figure 3. Ratio of 4s, 2s dome flats, displayed over range 1.9-2.1.

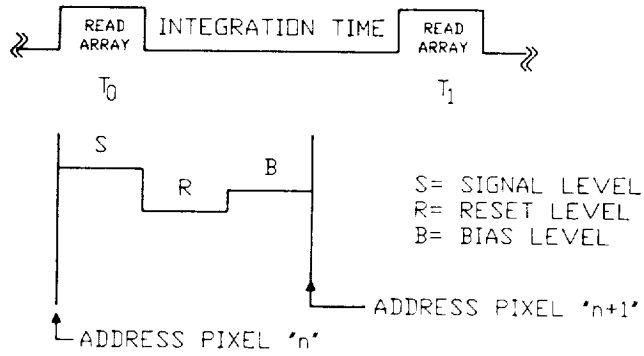

Figure 4a. Combined Readout

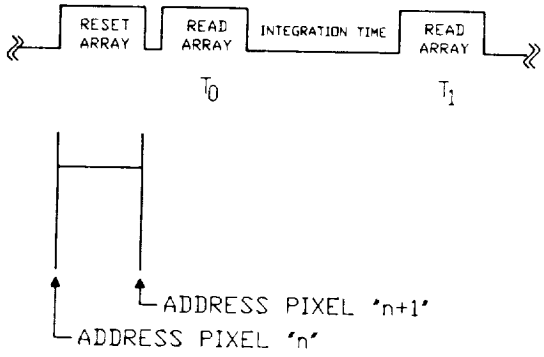

Figure 4b. Serial Readout

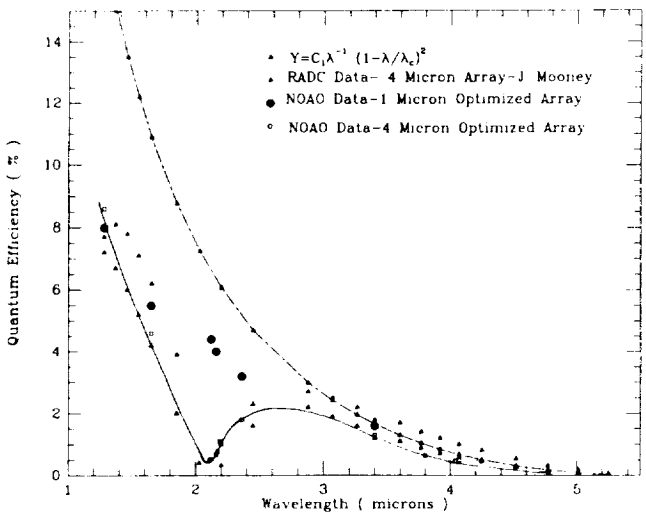

Figure 5. Quantum Efficiency

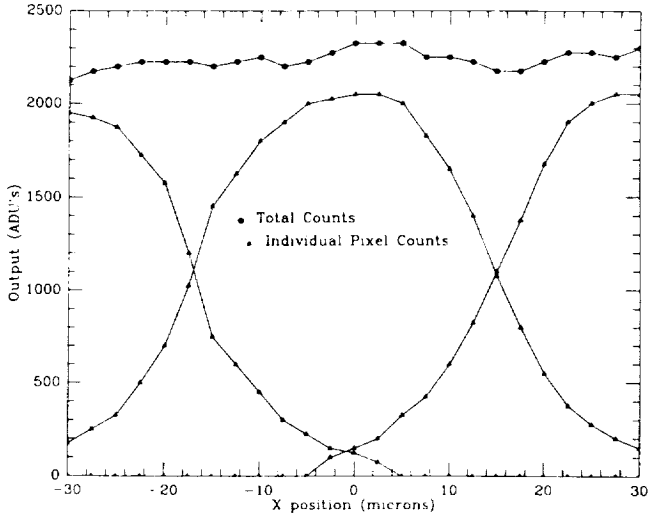

Figure 6. Spot Scan

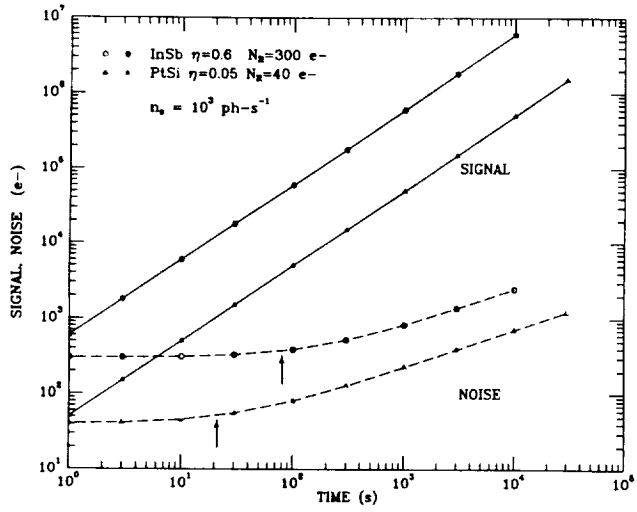

Figure 7a. Signal and Noise for InSb and PtSi

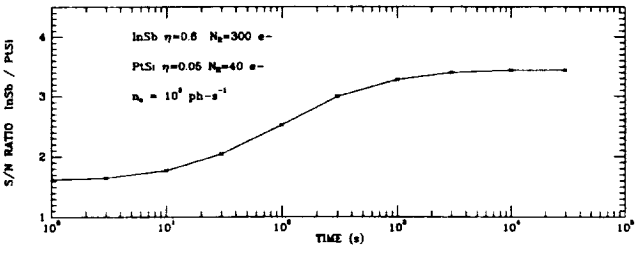

Figure 7b. Performance Ratio InSb/PtSi

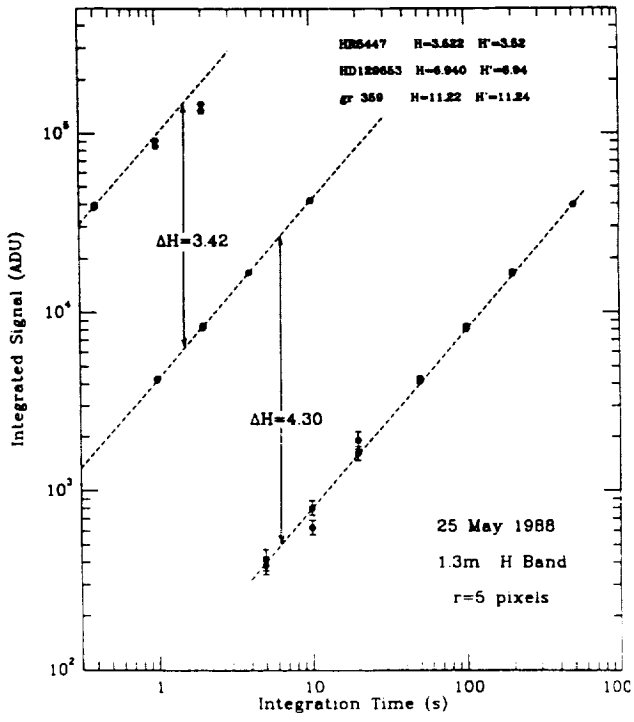

Figure 8. PtSi Linearity Observations

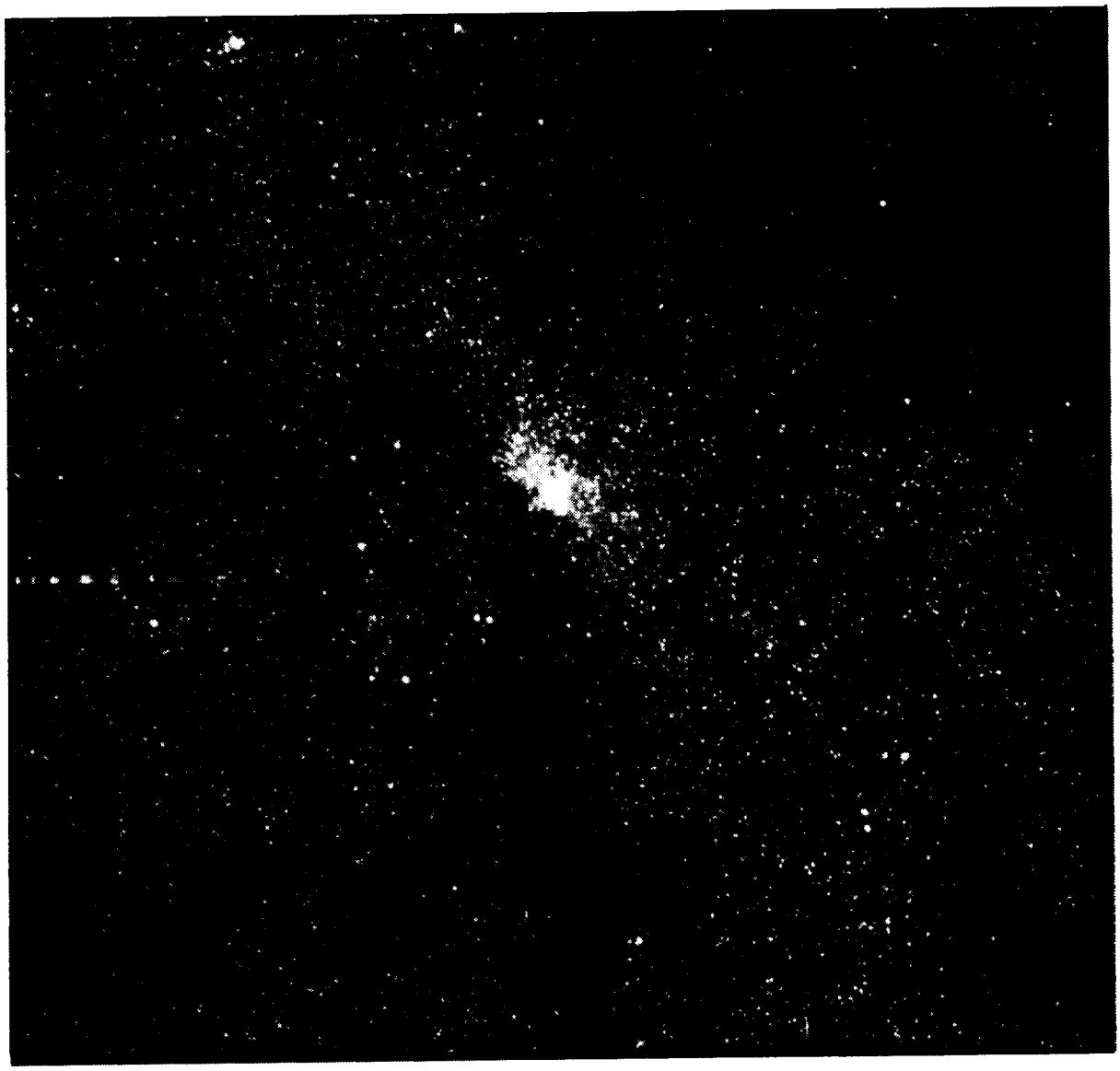

Figure 9 (above). K band mosaic of the galactic center. Field of view 27 arcmin square.

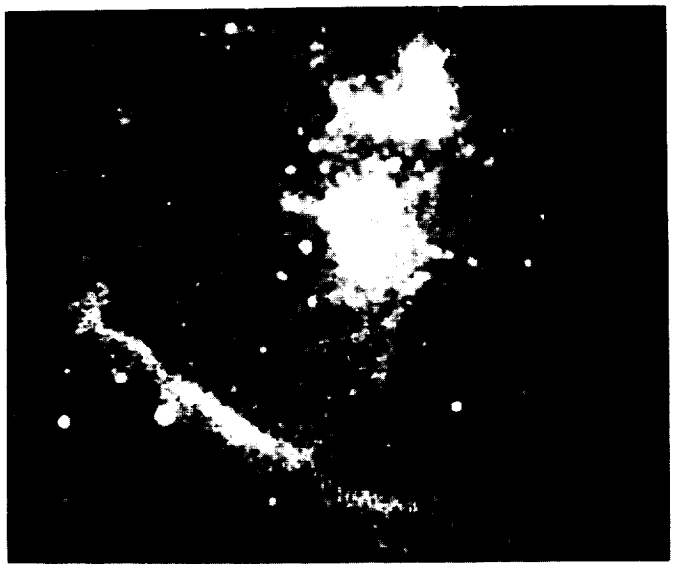

Figure 10 (left). Single frame image (6 arcmin square) of Orion Nebula, through a 3.28 micron ($\Delta\lambda$ = 0.1 micron) filter.

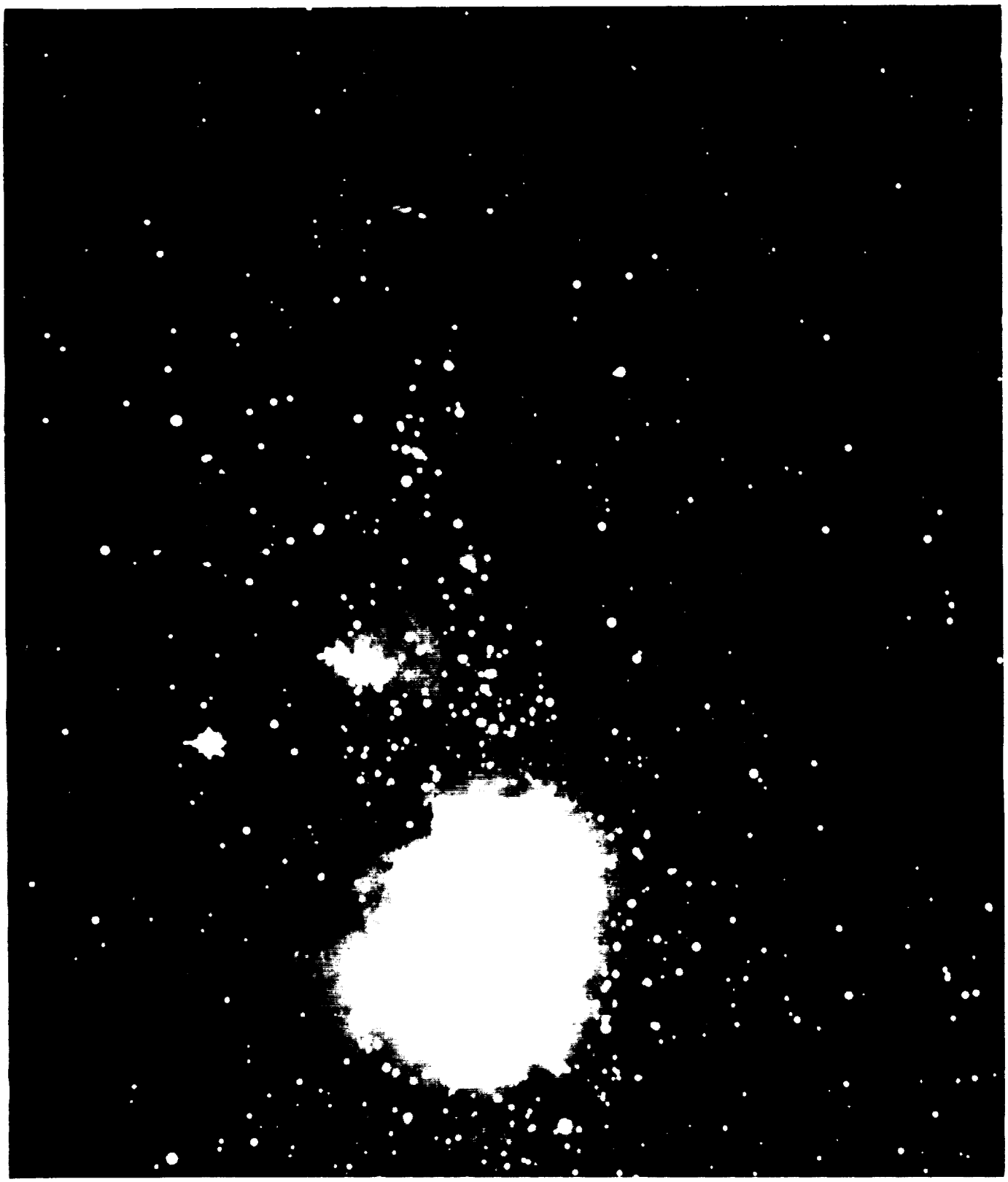

Figure 11. K band mosaic of the Orion Nebula. The field of view is approximately 27 x 37 arcmin.